Front. Mech. Eng. 2023, 18(1): 5
https://doi.org/10.1007/s11465-022-0721-3

RESEARCH ARTICLE

New nonlinear stiffness actuator with predefined torque–deflection profile

Wenjie JU[a], Hexi GONG[a], Keke QI[a], Rongjie KANG[a], Jian S. DAI[a,b,c], Zhibin SONG (✉)[a]

[a] *School of Mechanical Engineering, Tianjin University, Tianjin 300350, China*
[b] *College of Engineering, Department of Mechanical and Energy Engineering, Southern University of Science and Technology, Shenzhen 518055, China*
[c] *King's College London, University of London, WC2R 2LS London, UK*
✉ *Corresponding author. E-mail: songzhibin@tju.edu.cn (Zhibin SONG)*

ABSTRACT A nonlinear stiffness actuator (NSA) could achieve high torque/force resolution in low stiffness range and high bandwidth in high stiffness range, both of which are beneficial for physical interaction between a robot and the environment. Currently, most of NSAs are complex and hardly used for engineering. In this paper, oriented to engineering applications, a new simple NSA was proposed, mainly including leaf springs and especially designed cams, which could perform a predefined relationship between torque and deflection. The new NSA has a compact structure, and it is lightweight, both of which are also beneficial for its practical application. An analytical methodology that maps the predefined relationship between torque and deflection to the profile of the cam was developed. The optimal parameters of the structure were given by analyzing the weight of the NSA and the mechanic characteristic of the leaf spring. Though sliding friction force is inevitable because no rollers were used in the cam-based mechanism, the sliding displacement between the cam and the leaf spring is very small, and consumption of sliding friction force is very low. Simulations of different torque–deflection profiles were carried out to verify the accuracy and applicability of performing predefined torque–deflection profiles. Three kinds of prototype experiments, including verification experiment of the predefined torque–deflection profile, torque tracking experiment, and position tracking experiment under different loads, were conducted. The results prove the accuracy of performing the predefined torque–deflection profile, the tracking performance, and the interactive performance of the new NSA.

KEYWORDS compliant actuator, nonlinear stiffness actuator, nonlinear spring, predefined torque−deflection profile

1 Introduction

Compliance can offer greater shock tolerance, lower reflected inertia, more accurate and stable force control, and less inadvertent damage to the environment [1]. Owing to these advantages, compliant actuators have attracted increasing attention, especially in robotics in unstructured environments, such as walking robot [2], rehabilitation robot [3], prosthesis [4], and exoskeleton [5]. Compared with active compliant actuators, passive compliant actuators use practical elastic elements (such as springs) to interact with the environment, leading to intrinsic human/machine interaction safety, energy saving, and shock absorption [6].

Received January 20, 2022; accepted June 16, 2022

The study of passive compliant actuator could date back to the series elastic actuator (SEA) proposed by Pratt and Williamson [1] in 1995. This SEA is a linear metal spring in series with a stiff actuator. Next, SEAs with linear springs developed rapidly [7–13]. However, linear springs limit the performance of SEAs because of constant stiffness. For example, high stiffness increases control bandwidth and position tracking precision but reduces torque/force resolution and safety performance. Low stiffness increases torque/force resolution and shock absorption and improves safety performance at the cost of system control bandwidth [14–16]. Variable stiffness actuator (VSA) was proposed to overcome these limitations [17–30]. However, most VSAs (not including antagonistic compliant actuators) are equipped with two actuators (usually motors) to actively adjust stiffness and

equilibrium position independently, leading to bulky and complex structures and causing additional power consumption because of dedicated stiffness motor. Moreover, from the perspective of increasing torque resolution and bandwidth, complete decoupling of load and stiffness in VSAs results in some useless load–stiffness mapping space, where stiffness is high under small loads and stiffness is low under large loads. In addition, the speed of adjusting stiffness is usually limited by drive response and control efficiency, thus reducing interaction safety.

For optimization of the structure and control performance of VSAs, researchers designed nonlinear stiffness actuator (NSA), which is an SEA with a purely passive nonlinear spring that omits the active stiffness tuning motor at the cost of embedding a single load–deflection profile. The stiffness and equilibrium position of an NSA are coupled, and stiffness is adaptatively adjusted by load. The methods to achieve nonlinear stiffness considerably differ. Some researchers used commercially available off-the-shelf components, such as conical springs [31], "Jack Spring" [32], and compression spring [33], to achieve nonlinear stiffness. The use of off-the-shelf parts make these designs relatively inexpensive and easy to implement [15]. However, achieving diverse predefined load–deflection profiles is difficult.

Many researchers used assembled mechanical solutions to address the abovementioned limitations and achieve nonlinear stiffness. Thorson and Caldwell [34] designed an NSA that uses a hypocycloid mechanism to stretch a linear tension spring in a nonlinear manner. Chen et al. [35] used a gear and a pinion mechanism to compress compression springs in a nonlinear manner to perform nonlinear stiffness. Rodríguez et al. [36] designed an NSA, mainly including compliant beams and rollers. Li and Hao [37] and Liu et al. [38] used four-bar linkage mechanisms to achieve nonlinear stiffness. Li et al. [39] designed a spring-loaded inverted slider crank mechanism with nonlinear stiffness. However, these designs are not oriented to predefined torque–deflection profiles. Migliore et al. [40] used cams, rollers, and linear spiral springs to design a translational nonlinear stiffness mechanism, which could produce specific load–deflection relationships. Given that external force and spring force vectors are kept perpendicular, its dimension is difficult to be miniaturized. Shao et al. [41] designed a novel nonlinear spring mechanism with user-defined load–deflection behavior by combining a cam mechanism with parabolic beams. However, this mechanism is translational, which restricts the miniaturization of the prototype. Hao [42] proposed a general framework to design nonlinear compliant mechanisms with the desired nonlinear stiffness characteristics. For recent NSAs or nonlinear stiffness springs with predefined nonlinear stiffness characteristics, compactness is still a challenging issue.

For improvement of the compactness of existing assembled mechanical solutions, some researchers utilized the topology optimization method to achieve nonlinear stiffness. Palli et al. [43] used flexures to design a compliant element with a desired stiffness profile and range. Radaelli and Herder [44] implemented the shape optimization of compliant beams for prescribed load–displacement response. However, compared with analytical method, the topology optimization method is usually complex, and the actuator's performance critically depends on the accuracy of optimization method and the properties of selected materials.

Special materials could be used to achieve compact structure in NSAs. Schepelmann et al. [45] presented a compact nonlinear spring with a user-defined load–deflection profile by using rubber as the elastic element. However, its performance is partially compromised because of the hysteresis of the rubber material. Kuo and Deshpande [46] used compound mixed rubbers and a set of pulleys to design a small-sized robotic joint with nonlinear stiffness. Considering the stiffness property of the joint is closely related to the adjusted ratio of mixed compounds based on empirical trials and suggestions for manufacturing, precisely achieving diverse predefined load–deflection profiles is difficult. In addition, the aging of rubber limits the engineering application of these solutions. Leaf springs are widely used as compliant elements to achieve compact structure. Choi et al. [19] used leaf springs and rollers to design a robot joint. Bi et al. [47] proposed two compliant pivots, which used leaf springs to save structure space. Wu et al. [23] designed a leaf spring-based variable stiffness joint that has easy construction and large stiffness range.

Aside from the method to achieve nonlinear stiffness, the form of load–deflection profile for NSAs is an important issue. From the perspective of biomechanics and considering knee joint as an example, stiffness increases when knee joint moment increases [40]. The stiffness of soft tissues around human joints is nonlinearly related to the extent of stretch [48]. This finding implies a stiffening nonlinear coupling relationship between the joint stiffness and the external load; such relationship could be summarized as "low load, low stiffness and high load, high stiffness" [49]. In the authors' recent work [50], an optimal nonlinear stiffness design method for NSAs was proposed. The method could achieve a good trade-off between the bandwidth and the load resolution in human–robot interaction, not only proving the importance of nonlinear stiffness for a compliant actuator but also calculating an optimized nonlinear stiffness profile with a polynomial form.

On the basis of Ref. [50], using compliant beams, cams, and rollers, a design method for rotary NSAs with a predefined torque–deflection profile was proposed [51]. By using the abovementioned method, an NSA was designed, whose deflection range is restricted in ±1.7°

and stiffness range is 3.00–77.89 N·m/(°) [51]. Then, another design method for rotary NSAs with a user-defined torque–deflection profile was proposed utilizing torsional springs, cams, and rollers [52]. By using the proposed method, another NSA was designed, whose deflection range is restricted in ±2° and stiffness range is 0.93–36.21 N·m/(°). However, the compactness of the abovementioned NSAs could still be improved.

According to the above analysis, designing an NSA with predefined stiffening torque–deflection, which is easy to implement, compact, and light, is still challenging. In this paper, oriented to engineering applications, a new simple NSA was proposed, including leaf springs and especially designed cams, and it could perform a predefined stiffening torque–deflection profile. Moreover, the new NSA has a compact structure, and it is lightweight, which are both beneficial for its practical application. The remainder of this paper is organized as follows. Section 2 describes the principle of the new NSA. In Section 3, the optimal design parameters are given by analyzing the weight of the NSA and the mechanic characteristic of the leaf spring. In Section 4, the sliding displacement between the cam and the leaf spring and the consumption of it were calculated to evaluate the influence of sliding friction force. Section 5 presents the mechanical design of the NSA. Simulations and prototype experiments are detailed in Section 6, along with the results showing the effectiveness and control performance of the new NSA. In Section 7, the advantages and limitations of this study are discussed. Finally, the conclusions of this study are presented in Section 8.

2 Principle of the new NSA

NSA is typically composed of a motor (usually with a reducer), a nonlinear spring mechanism, and an output link, as shown in Fig. 1(a). When the external torque τ is zero, the motor and the output rotate for the same angle. When the external torque τ is not zero, the motor rotates for θ_m, but the output rotates for θ_e. The difference between θ_m and θ_e is the very deflection α of the nonlinear spring and the NSA, which is related to τ nonlinearly. The relationship among α, θ_m, and θ_e is shown in Fig. 1(b).

2.1 Configuration of nonlinear spring

Nonlinear spring is the key part of the NSA, and it is fundamental to perform nonlinear stiffness. In this study, a new cam-based mechanism, as indicated by the red dotted rectangle in Fig. 2(a), was proposed to achieve nonlinear stiffness, and multiple identical cam-based

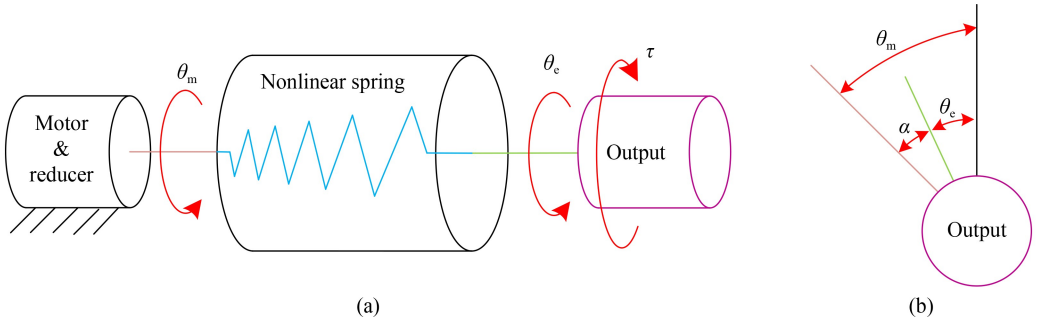

Fig. 1 Configuration of nonlinear stiffness actuator: (a) principle block diagram and (b) side view.

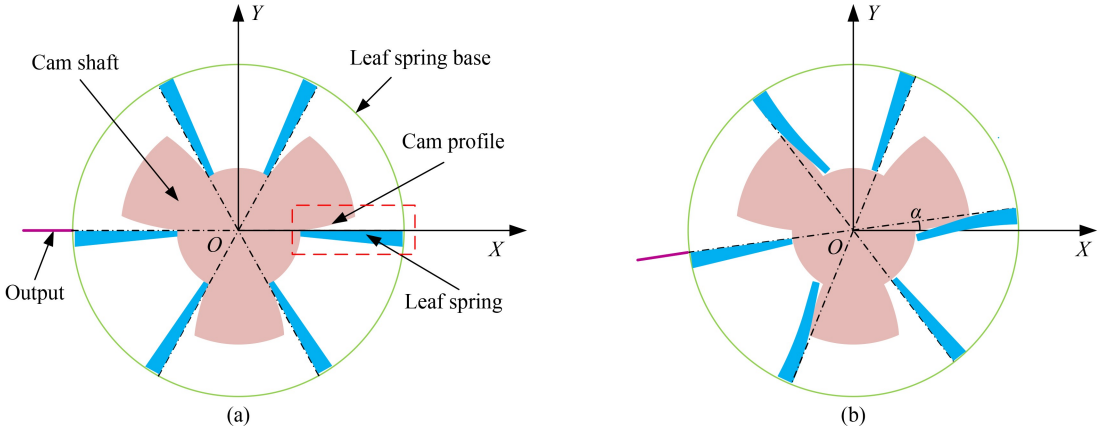

Fig. 2 Configuration of nonlinear stiffness actuator: (a) undeflected nonlinear spring and (b) nonlinear spring deflected for α.

mechanisms were arranged to design the nonlinear spring. In particular, the roller was abandoned in the cam-based mechanism considering that the roller limits miniaturization. In a single rotational direction, multiple cam-based mechanisms were circumferentially and uniformly distributed to reduce the strength requirement of leaf springs, and the same number of cam-based mechanisms was arranged alternatively in the opposite rotational direction to achieve bidirectional stiffness characteristics.

The proposed nonlinear stiffness spring is mainly composed of a cam shaft, multiple leaf springs, a leaf spring base, and an output link, as shown in Fig. 2. One end of a leaf spring is rigidly embedded in the leaf spring base, whereas the other end is free. The output link is rigidly mounted on the leaf spring base. The path of torque transferring is as follows. When the motor drives the cam shaft to rotate, the leaf springs, leaf spring base, and output passively rotate, which is coaxial with the cam shaft. Given that the cam shaft, leaf spring base, and output are rigid but the leaf springs, which act as cantilevers, are compliant, the leaf springs deflect under the torque.

In general, the nonlinearity of the proposed NSA arises from the change in the effective length of the leaf spring in the cam-based mechanism. One cam-based mechanism consists of a leaf spring and an especially designed cam. Assuming that the cam shaft is fixed, when no external torque is applied to the output, the cam shaft and output do not rotate relatively, and the leaf springs remain straight, as shown in Fig. 2(a). However, when an external torque is applied to the output anticlockwise, the cam shaft and output rotate relatively to make the leaf spring deform; thus, the nonlinear spring deflects for α, as shown in Fig. 2(b). When the external torque varies from zero to the maximum, the nonlinear spring also deflects from zero to the maximum. Meanwhile, the contact point (which is a line) between the leaf spring and the cam moves along the cam profile, leading to a variation in the stiffness of the nonlinear spring. By purposely designing the cam profile curve to adjust the effective length of the leaf spring, a desired nonlinear stiffness characteristic could be achieved.

As shown in Fig. 2, to make full use of the strength of the leaf spring, its longitudinal section is varied, and its contact plane with the cam is arranged vertically to its cross section. In this study, a leaf spring with a right trapezoid longitudinal section was used. The origin of the Cartesian coordinate system is at the rotational center O of the cam shaft, with the X and Y axes along the horizontal and vertical directions, respectively. With the cam-based mechanism in the red dotted rectangle in Fig. 2(a) as an example, when the external torque is zero, the contact plane of the leaf spring, the symmetric plane of the cam shaft, and the X axis have a coplanar arrangement.

2.2 Design of cam profile curve

The primary challenge in designing an NSA is to design the cam profile curve of the cam-based mechanism. The static analysis diagram of the cam-based mechanism is shown in Fig. 3, and it corresponds to the cam-based

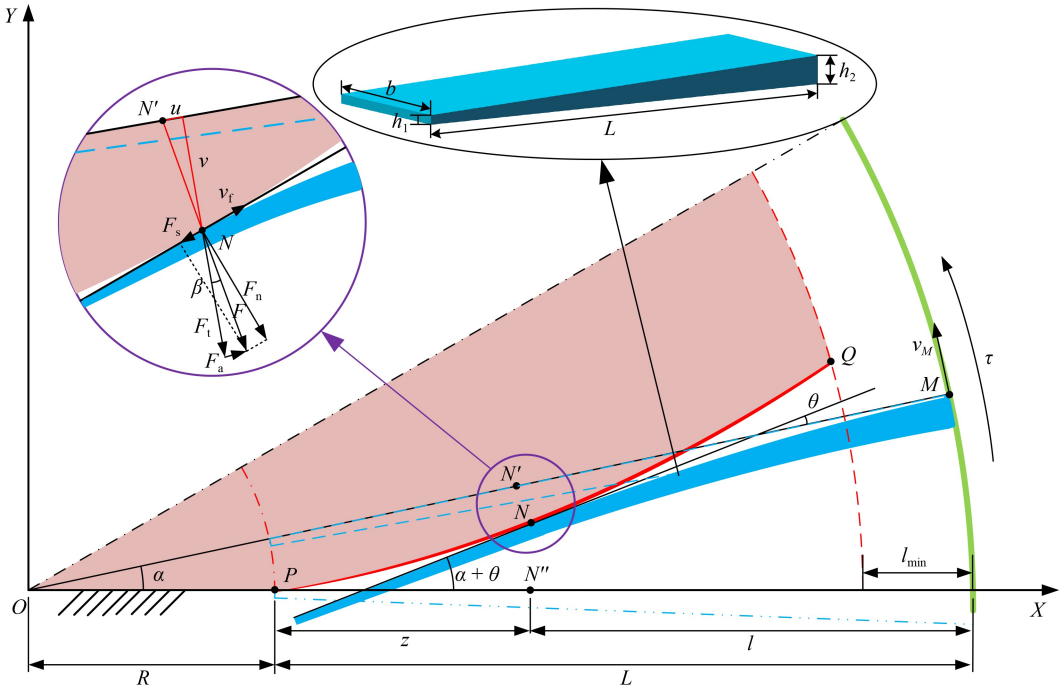

Fig. 3 Static analysis diagram of the cam-based mechanism. The dull red shape denotes the cam shaft, and the bold red line represents the cam profile. The blue shape denotes the leaf spring. The green shape is the leaf spring base.

mechanism in the red dotted rectangle in Fig. 2(a). When the external torque τ is zero, no contacting force could be observed between the cam and the leaf spring, and the point P (which is actually a line) on the cam profile contacts the free end of the leaf spring. When the external torque τ is maximum, the contacting force between the cam and the leaf spring is maximum, and the leaf spring deforms to contact the cam profile on point Q. When the external torque τ increases from zero to the maximum, the leaf spring deforms under the contacting force F, and the contact point N on the cam profile changes from point P to point Q. As a result, the track of point N is the very cam profile curve, which maps the predefined torque–deflection profile. A notable detail is that only the effective part of the leaf spring deforms, which is from the contact point N to its fixed end. As shown by the purple circle in Fig. 3, the contacting force F applied to the leaf spring is composed of the sliding friction force F_s and the normal force F_n. However, to formulate the deflection of the leaf spring, F is decomposed into the tangential component F_t and axial component F_a. F_t is vertical to the cross section of the leaf spring, whereas F_a is tangential to it.

Before derivation, the design parameters of nonlinear spring are given, including R, L, b, h_1, and h_2, where R is the distance between points O and P. The geometry of the leaf spring is shown in the black ellipse in Fig. 3, where L and b are the length and width of the leaf spring, respectively, and h_1 and h_2 are the heights of the free end and fixed end of the leaf spring ($h_2 \geqslant h_1$), respectively. According to the coordinate transformation, when point N on the leaf spring contacts the cam, point N is assumed to be transformed from point N'' to point N' to point N. Specifically speaking, point N'' on the leaf spring rotates by α to point N', and then point N' on the leaf spring deforms tangentially by v under F_t and offsets axially by u under F_a to point N. As the axial offset u of the leaf spring is negligible compared with the tangential deformation v of the leaf spring, the coordinate transformation formula from point N'' to point N is given as follows:

$$\begin{bmatrix} x_N \\ y_N \end{bmatrix} = \begin{bmatrix} \cos\alpha & -\sin\alpha \\ \sin\alpha & \cos\alpha \end{bmatrix} \begin{bmatrix} x_{N''} \\ y_{N''} \end{bmatrix} + \begin{bmatrix} v\sin\alpha \\ -v\cos\alpha \end{bmatrix}, \tag{1}$$

where (x_N, y_N) and $(x_{N''}, y_{N''})$ are the coordinates of points N and N'', respectively. The sign of α is "+." The unit of α is "°."

Assuming that the effective length of the leaf spring is l and l is known, the coordinates of point N'' are $(L + R - l, 0)$. By substituting the coordinates of point N'' into Eq. (1), the coordinates of N could be expressed as follows:

$$\begin{bmatrix} x_N \\ y_N \end{bmatrix} = \begin{bmatrix} (L+R-l)\cos\alpha + v\sin\alpha \\ (L+R-l)\sin\alpha - v\cos\alpha \end{bmatrix}. \tag{2}$$

The tangential deformation v and the deflection angle θ of the leaf spring with length l are expressed as follows:

$$v = \int_0^l \frac{F_t z^2}{EI_z}\mathrm{d}z + \xi\int_0^l \frac{F_t z}{GA_z}\mathrm{d}z, \tag{3}$$

$$\theta = \int_0^l \frac{F_t z}{EI_z}\mathrm{d}z, \tag{4}$$

where z is the distance of a point to free end on the leaf spring and $0 \leqslant z \leqslant l$, I_z and A_z are the moment of inertia and the area of the cross section, respectively, whose distance to the free end of the leaf spring is z, ξ is a coefficient related to the uniform distribution of the shear stress, which is 1.2 when the longitudinal section of the leaf spring is a right trapezoid, and E and G are the Young's modulus and shear modulus of the leaf spring, respectively. The unit of θ is "rad."

According to the arrangement of leaf springs, I_z and A_z could be calculated as follows:

$$I_z = \frac{bh_1^3}{12}\left(1 + \left(\left(\frac{h_2}{h_1}\right) - 1\right)\frac{z}{l}\right)^3, \tag{5}$$

$$A_z = \frac{bh_1}{12}\left(1 + \left(\left(\frac{h_2}{h_1}\right) - 1\right)\frac{z}{l}\right). \tag{6}$$

The external torque τ could be obtained as follows:

$$\tau = n[F_t(L+R-l) + F_a v], \tag{7}$$

where n is the count of leaf springs in a single rotational direction.

F_a could be obtained by

$$F_a = F_t \tan\beta, \tag{8}$$

where β is the angle between F_a and F_t. Under the small deformation hypothesis, β is small, so F_a is very small with respect to F_t.

Considering that v is negligible compared with $(L + R - l)$, τ could be approximated as follows:

$$\tau = nF_t(L+R-l). \tag{9}$$

As the external torque τ is predefined, F_t could be calculated as

$$F_t = \frac{\tau}{n(L+R-l)}. \tag{10}$$

Thus far, if only l is solved, the coordinates of point N could be solved. In this study, the coordinates of point N and the cam profile were solved using a discrete and iterative method. The total deflection α is assumed to be divided into c uniform intervals. Therefore, the contacting point varies from point P to point Q for α/c per interval. In the mth interval ($1 \leqslant m \leqslant c$), α, θ, and the coordinates of point N satisfy the following relationship:

$$\tan\left(\frac{\pi\alpha}{180} + \theta\right) = \frac{y_N - y_{N_f}}{x_N - x_{N_f}}, \tag{11}$$

where x_{N_f} and y_{N_f} are the coordinates of point N_f, which represents the former contact point before point N.

In the first interval, point N_f is the same as point P, and its coordinates are (R, 0). By combining Eqs. (2)–(6), (10), and (11) and the coordinates of point P, the value of l could be solved. Then, the coordinates of point N could be solved by substituting the value of l into Eqs. (2), (3), (5), (6), and (10). Next, by updating point N_f with point N and repeating the method used in the previous interval, the second point N could be obtained. By iterating c times, a series of discrete points on the cam profile curve could be obtained. Finally, the cam profile curve could be obtained using a smooth curve to fit those discrete points. The value of c is positively correlated with the precision of the cam profile curve but negatively correlated with the calculative efficiency.

On the condition that L, R, b, h_1, and h_2 are given, the solving method of the cam profile curve is derived. The values of L, R, b, h_1, and h_2 are still needed to obtain a feasible cam profile. According to the configuration, (L + R) and b are closely related to the radial and axial dimensions of the NSA, respectively, which could be predetermined in accordance with the dimension requirements for application scenarios. Considering that a too-small h_1 is restricted by the machining precision and could affect the strength of the entire leaf spring, h_1 is predetermined. Therefore, only L, R, and h_2 are not known. In this study, L, R, and h_2 could be solved using the minimum stiffness of the NSA, which could be obtained by taking the derivative of the predefined torque–deflection profile with respect to the deflection and setting deflection as zero.

The minimum stiffness of the NSA is the stiffness on point P, as shown in Fig. 3, which could be derived using the method on the basis of Fig. 4. The coordinates are set same as those in Fig. 3. The cam could be assumed to always contact the leaf spring in point P when the deflection of the nonlinear spring is very small. The detailed derivation of the minimum stiffness k_{min} is as follows:

$$v = R\sin\alpha, \tag{12}$$

$$L + R = l + R\cos\alpha. \tag{13}$$

When the output revolves around the cam shaft, the contact point in the leaf spring varies slightly. Therefore, the height of the leaf spring (h) at the contact point becomes

$$h = h_2 - \frac{l(h_2 - h_1)}{L}. \tag{14}$$

The external torque τ could be approximated by

$$\tau = nF_t R\cos\alpha. \tag{15}$$

By combining Eqs. (3), (5), (6), and (12)–(15), τ could be expressed as follows:

$$\tau = f_1(\alpha, L, R, h_2), \tag{16}$$

where $f_1(\cdot)$ is a function of α, L, R, and h_2.

By taking the derivative of τ with respect to α and then setting α to zero, α is eliminated, and k_{min} could be expressed as follows:

$$k_{min} = f_2(L, R, h_2), \tag{17}$$

where $f_2(\cdot)$ is a function of L, R, and h_2, and the unit of k_{min} is "N·m/(°)."

Given that (L + R) is predetermined, the corresponding L could be solved by listing the possible values of R. Then, h_2 could be solved by substituting the values of k_{min}, R, and L into Eq. (17). By using the preceding method, many groups of feasible L, R, and h_2 are presented.

A flowchart is presented in Fig. 5 to clearly demonstrate the design process of the cam profile curve.

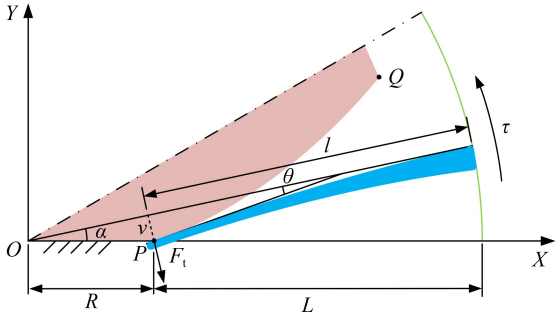

Fig. 4 Schematic used for deriving the minimum stiffness of nonlinear stiffness actuator.

3 Analysis and determination of the design parameters of nonlinear spring

On the condition that the dimension requirements of the NSA are known, many groups of design parameters are obtained. However, to improve the practicability of the proposed design, choosing the optimal design parameters is necessary. In this study, an analytical method was adopted to determine the optimal design parameters of the nonlinear spring.

A predefined stiffening nonlinear torque–deflection profile, which has a form similar to the optimal profile in the recent work [50], was adopted to emulate the characteristics of skeletal muscle. The predefined torque–deflection profile of the NSA is given by

$$\tau = 0.687\alpha^3 + 0.213\alpha^2 + 0.18\alpha. \tag{18}$$

Not like many other compliant actuators, which have large deflection ranges, the deflection range α is constricted as ±3°, and the reasons are as follows. First, for the predefined torque–deflection profile with a monotone increasing polynomial form, when the torque range is decided, a small deflection range is beneficial for achieving a bigger stiffness, which could increase the control bandwidth of the NSA. Second, a small deflection range is beneficial for minimizing the effect of sliding friction force because of eliminating the roller.

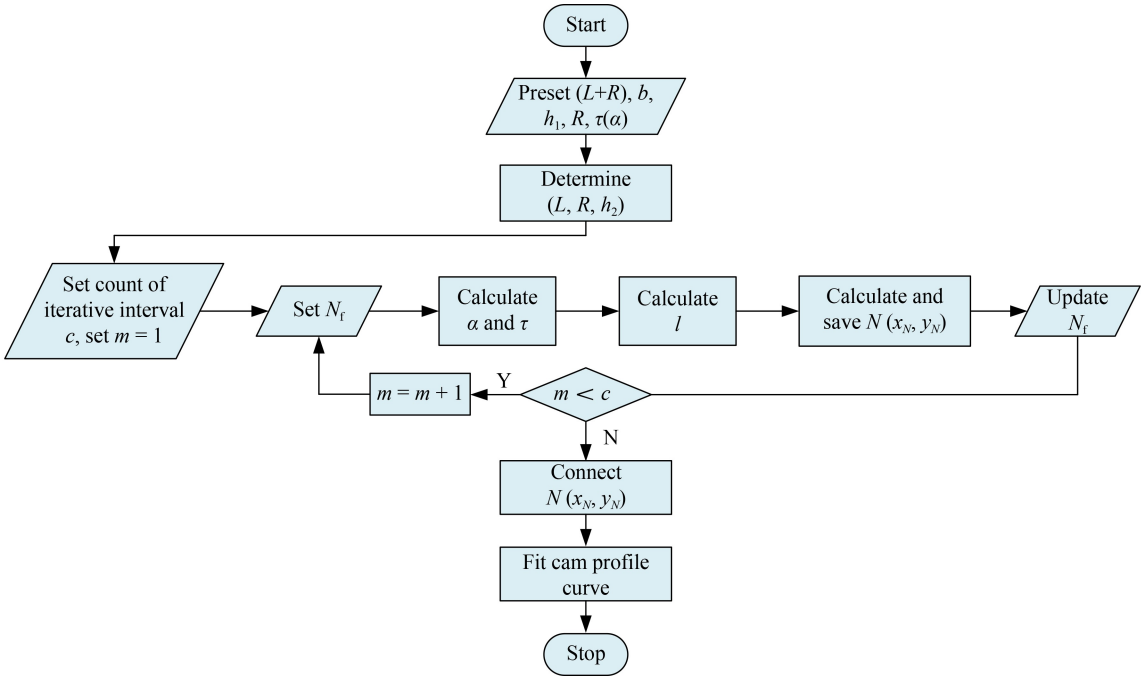

Fig. 5 Flowchart of the design process of cam profile curve.

(L + R) is 31 mm, and b is 21 mm. The material of the leaf spring is 60 Si_2Mn, which has a Young's modulus of 206 GPa, shear modulus of 79 GPa, and Poisson's ratio of 0.3. The material of cam shaft is alloy steel with a density of 7850 kg/m^3. Considering the calculative accuracy and efficiency, the count of the iteration is 400.

3.1 Analysis of design parameters of nonlinear spring

3.1.1 Influence on the weight of cam

Although the dimension of the nonlinear spring is predetermined, different design parameters lead to different weights of the NSA. Therefore, the influence of design parameters on the weight of the NSA must be studied. In this work, the weight difference of NSAs with different design parameters is in nonlinear spring. As (L + R) and b are predetermined, the weight of the leaf spring base is almost fixed. When the height of leaf spring is small, its weight is negligible compared with that of cam shaft. Therefore, the weight difference resulting from different design parameters is mainly influenced by the cam shaft, especially the cam. Considering that the curvature of the cam is large, the weight of the cam D_{cam} could be estimated as follows:

$$D_{\text{cam}} = \frac{\rho b\left[\pi(L+R-l_{\min})^2+\pi R^2\right]}{2}, \tag{19}$$

where ρ is the density of cam shaft, and $l_{\min}$ is the minimum value of l, which can be estimated using the l in Q, as shown in Fig. 3.

As shown in Eq. (19), the weight of the NSA is influenced by R and $l_{\min}$. However, considering that $l_{\min}$ is calculated using R and h_1, the influence of R and h_1 on D_{cam} was investigated. The results are presented in Fig. 6(a). The weight of the NSA increases with R and h_1. Therefore, from the perspective of lightweight, a small R and a small h_1 should be selected when designing the NSA.

3.1.2 Influence on the strength of leaf spring

The strength of the leaf spring affects the overload capacity of the NSA. Under the condition that the height of the leaf spring at the free end is not too small, the strength of the leaf spring is mainly restricted by the maximum normal stress σ on the fixed end when the bending moment on the leaf spring is maximum. σ should satisfy the strength criterion:

$$\sigma = \frac{M_{\max}}{W} \leqslant [\sigma], \tag{20}$$

$$W = \frac{bh_2^2}{6}, \tag{21}$$

where $M_{\max}$ is the maximum bending moment in the leaf spring, which could be estimated by Eq. (22), W is the section modulus on the fixed end of the leaf spring, and $[\sigma]$ is the permissible bending stress of the leaf spring.

$$M_{\max} = \frac{\tau_{\max} l_{\min}}{L+R-l_{\min}}, \tag{22}$$

where $\tau_{\max}$ is the maximum torque applied to the NSA, which could be determined by the predefined torque–deflection profile.

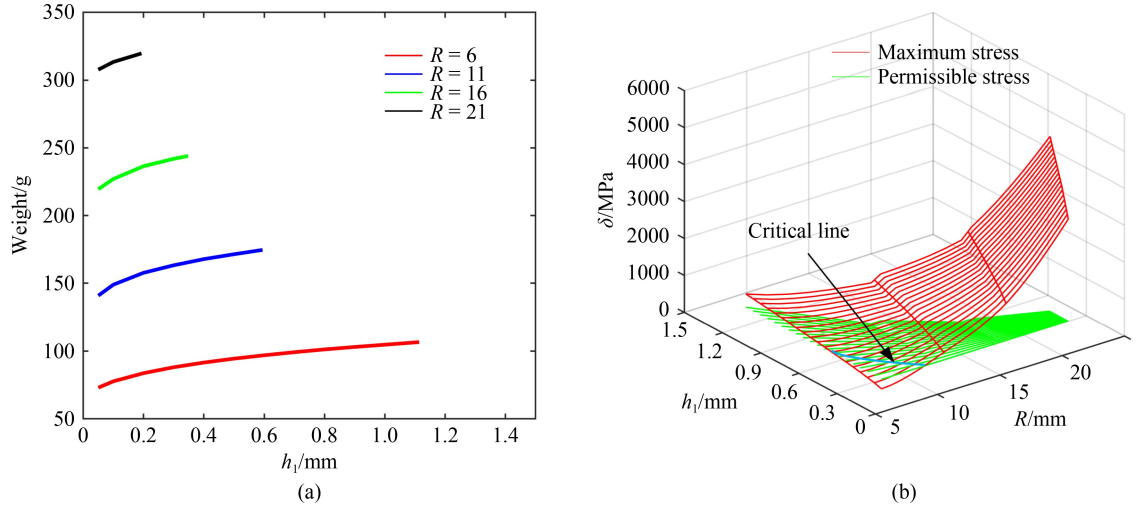

Fig. 6 Influence of R and h_1 on (a) the weight of cam and (b) the strength of leaf spring.

The influence of R and h_1 on the strength of the leaf spring was investigated, and the results are presented in Fig. 6(b). The design parameters that make the maximum normal stress below the permissible stress surface are available, and the critical line is shown by the blue line. With an increase in R and h_1, the maximum normal stress in the leaf spring increases. In particular, when R is large, the normal stress in the leaf spring increases sharply with an increase in h_1. As a result, to enhance the overload capacity of the NSA, a small R and a small h_1 should be selected.

3.2 Determination of design parameters

According to the preceding analysis, a small R and a small h_1 should be used to design the NSA. In this study, the minimum value of R, which is restricted by the strength of the cam shaft, was selected. With regards to h_1, a too small value may increase manufacturing difficulty, and the stress at the free end of the leaf spring may cause problems. The design parameters were determined under comprehensive consideration, as shown in Table 1.

4 Sliding friction force analysis in nonlinear spring

Compared with the NSA proposed previously [51,52], the new NSA uses cams and leaf springs without rollers to transmit torque. Therefore, sliding friction force is an inevitable issue. The sliding distance and consumption of sliding friction force were calculated using the discrete method described in Section 2 to evaluate the effect of sliding friction force on the new NSA.

Table 1 Design parameters of nonlinear spring

Parameter	Value/mm
L	25.0
R	6.0
h_1	0.4
h_2	1.5
b	21.0

4.1 Sliding distance of leaf spring

The sliding distance of leaf spring in a cam-based mechanism is the same as the sliding distance in NSA. For a cam-based mechanism, the sliding distance in the mth interval is the difference between the length of the cam profile and the effective length variation of leaf spring in the mth interval. Although the cam profile is an arc, the length of the cam profile curve s_{cm} in the mth interval could be estimated by the straight-line length in the mth interval when the interval is sufficiently small.

$$s_{cm} = \sqrt{(x_m - x_{m-1})^2 + (y_m - y_{m-1})^2}, \tag{23}$$

where (x_m, y_m) and (x_{m-1}, y_{m-1}) are the coordinates of the mth and $(m-1)$th points on the cam profile curve, and (x_0, y_0) are $(R, 0)$ when m is 1.

The effective length variation s_{lm} of the leaf spring in the mth interval is given by

$$s_{lm} = l_m - l_{m-1}, \tag{24}$$

where l_{m-1} is the effective length of the leaf spring on the $(m-1)$th contact point, and l_0 is L when m is 1.

The sliding distance of the leaf spring s_{rm} (relative displacement) in the mth interval is

$$s_{rm} = s_{cm} - s_{lm}. \tag{25}$$

The accumulated sliding distance S_r (relative displacement) of leaf spring with an increase of α is

$$S_r = \sum_{m=1}^{c} s_{rm}. \tag{26}$$

The accumulated sliding distance of the leaf spring is shown in Fig. 7(a). This sliding distance increases faster with the increase in deflection, indicating that the sliding speed increases. However, the sliding distance and sliding rate are negligibly small.

4.2 Consumption of sliding friction force

The power of the sliding friction force P_s in the nonlinear spring could be calculated as follows:

$$P_s = nF_s v_s, \tag{27}$$

where v_s is the sliding velocity, and F_s is the sliding friction force.

The external torque τ could be obtained by

$$\begin{aligned}\tau = {} & nF_n((L+R-l-v\tan\theta)\cos\theta) \\ & + F_s((L+R-l-v\tan\theta)\sin\theta + v/\cos\theta).\end{aligned} \tag{28}$$

In this paper, F_s could be estimated by the following:

$$F_s = \mu F_n, \tag{29}$$

where μ is the coefficient of sliding friction force.

As shown in Fig. 3, the sliding velocity v_s could be approximated by the projection of the velocity of point M on the direction of v_s as follows:

$$v_s = v_M \sin\theta, \tag{30}$$

where v_M is the velocity of point M and could be obtained by

$$v_M = \omega(L+R), \tag{31}$$

where ω is the angular velocity of the spring base. Here, it was set to 1 rad/s.

The power of the external torque (P_τ) is given by

$$P_\tau = \omega\tau. \tag{32}$$

The powers of the sliding friction force and external torque in the NSA were calculated, as shown in Fig. 7(b). Although no roller is present, the value and percentage of the sliding friction force power are very small compared with the power of the external torque, indicating low consumption of the sliding friction force in the nonlinear spring. Moreover, considering that the deformation of the leaf spring is small, the mechanical efficiency of the nonlinear spring could be evaluated by the percentage of the sliding friction force power on the external torque power. The mechanical efficiency of the nonlinear spring is high.

5 Mechanical design of NSA

In this section, a prototype of the NSA, where the cam profile curve of cam was calculated using the design parameters in Table 1, is described. As shown in Fig. 8, the mechanical structure of the NSA is mainly composed of a nonlinear spring, a motor, and a reducer. The nonlinear spring is mainly composed of a leaf spring base, a cam shaft, six identical leaf springs, and an output link. A rotatory encoder was used with its kinetic disk mounted on the output link and static disk mounted on the cam shaft to measure the deflection of the NSA. The leaf spring is fixed in a slot inside the leaf spring base, and it is axially fixed by two bolts and circumferentially fixed by one gasket and two jackscrews. The output link could be used not only to transmit external torque but also to support the cam shaft. Holes are processed on the side of the cam shaft to reduce the weight of the cam shaft.

6 Simulations and experiments

6.1 Simulations of torque–deflection profiles

In addition to the profile expressed by Eq. (18), two more

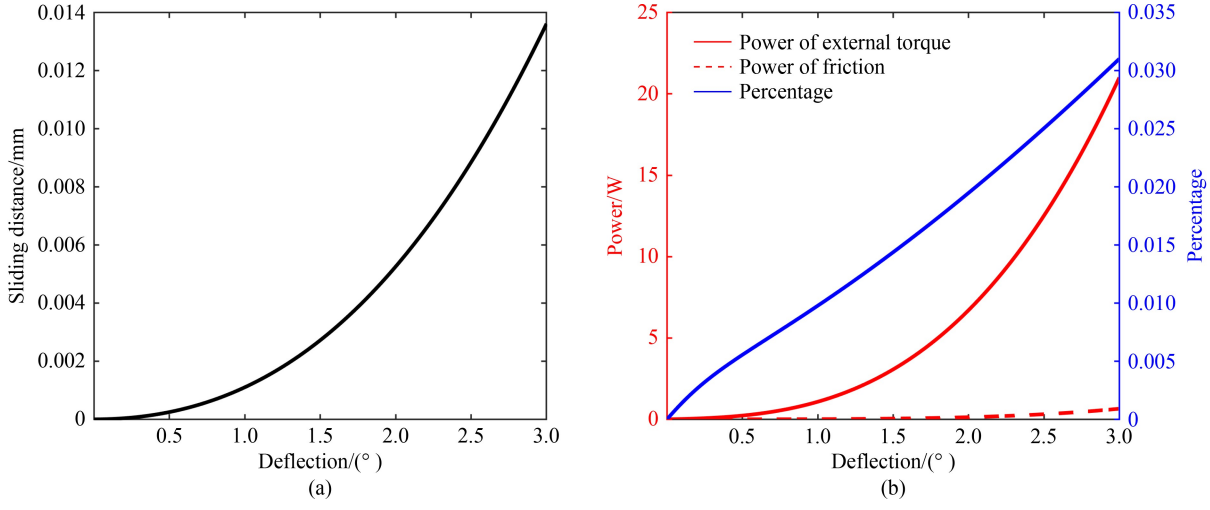

Fig. 7 Influence of sliding friction force on nonlinear spring: (a) accumulated sliding distance of leaf spring and (b) powers of the sliding friction force and external torque and their percentage.

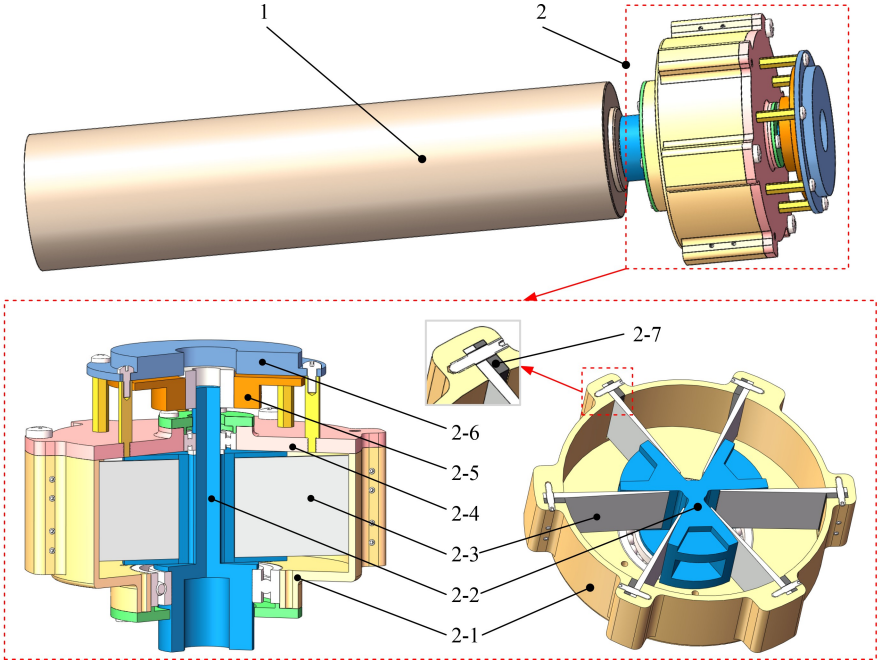

Fig. 8 Three-dimensional model of the nonlinear stiffness actuator. 1: motor and reducer, 2: nonlinear spring, 2-1: leaf spring base, 2-2: cam shaft, 2-3: leaf spring, 2-4: output, 2-5: static disk of encoder, 2-6: kinetic disk of encoder, and 2-7: gasket.

torque–deflection profiles expressed by Eqs. (33) and (34) were selected for simulations to verify the accuracy and applicability of the nonlinear spring. For comparison and observation, the deflection ranges, torque ranges, and initial stiffnesses of three torque–deflection profiles are similar (±3°, 0–21 N·m, and 0.18 N·m/(°), respectively), and the design parameters of nonlinear springs are identical, as presented in Table 1. The stiffness curves of these three predefined torque–deflection profiles are shown in Fig. 9(a). Considering that the stiffness characteristics of the NSA in two rotational directions are identical, the simulation results for only one direction are shown here for brevity.

$$\tau = 0.415\alpha^4 - 2.22\alpha^3 + 5.19\alpha^2 + 0.18\alpha, \quad (33)$$

$$\tau = -0.141\alpha^3 + 2.7\alpha^2 + 0.18\alpha. \quad (34)$$

On the basis of the proposed method in this study, the cam profile curves were solved, as shown in Fig. 9(b). The three-dimensional models of nonlinear springs were developed and imported into simulation software to perform simulations. The sliding friction force between the leaf springs and the cams were considered in the simulation. The simulation results and errors are shown in Figs. 9(c)–9(e). Compared with the predefined torque–deflection profiles, the simulated values show good agreement. In the loading phase, when the external torque increases from zero to the maximum value, the maximum errors are −0.359, 0.364, and 0.448 N·m, and the root mean square (RMS) errors are 0.108, 0.200, and 0.175 N·m, respectively. In the unloading phase, when the external torque decreases from the maximum value to zero, the maximum errors are −0.436, 0.357, and 0.441 N·m, and the RMS errors are 0.131, 0.213, and 0.188 N·m, respectively. Errors mainly arise from the iteration error and sliding friction force between cams and leaf springs. From the error graphs, in the unloading phase, the nonlinear spring shows slight torque hysteresis because of the sliding friction force. However, the hysteresis is small because the moment arm of the sliding friction force nearly passes through the rotational center of the nonlinear spring. Thus, the torque induced by the sliding friction force is small. In conclusion, the proposed nonlinear spring could realize different torque–deflection profiles of “low load, low stiffness and high load, high stiffness” precisely.

6.2 Verification experiment of the predefined torque–deflection profile

A prototype of the new NSA was fabricated to further verify the accuracy of the nonlinear spring for performing the predefined torque–deflection profile, as shown in Fig. 10, and it has the profile in Eq. (18). A Maxon DC motor (RE40 148867) and a reducer (80:1) were used to actuate the nonlinear spring. An absolute encoder (Encoder 1) was installed on the tail of the motor to measure the position of the input of the NSA. A capacitive absolute encoder (Encoder 2) was installed to measure the deflection of the NSA. The cam profile is shown by the red dotted rectangle in Fig. 10(c). Considering that the nonlinear spring is universal by

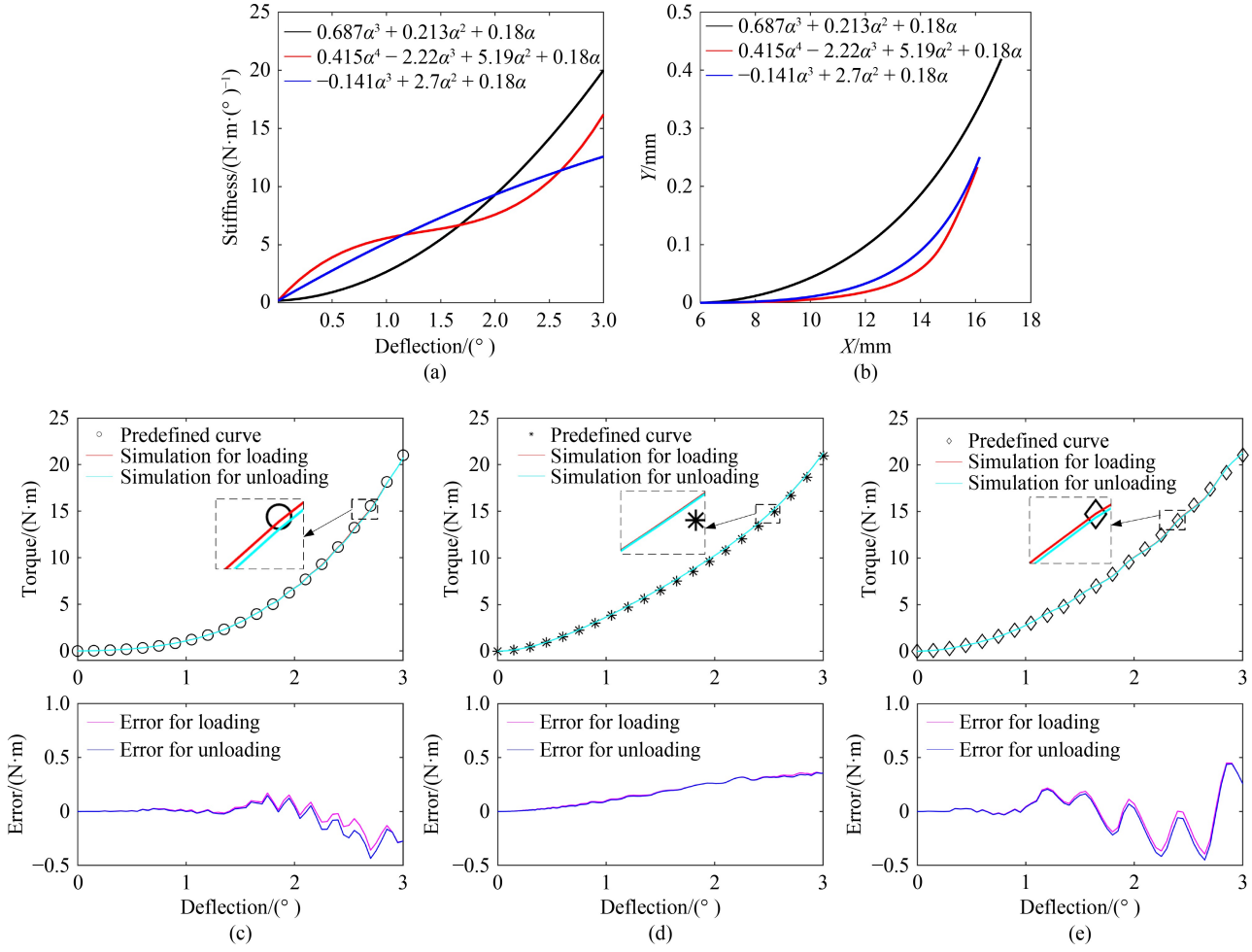

Fig. 9 Simulations of nonlinear springs with different torque–deflection profiles: (a) stiffness curves, (b) calculated cam profile curves, comparison between simulated curve with predefined profile for (c) $(0.687\alpha^3 + 0.213\alpha^2 + 0.18\alpha)$, (d) $(0.415\alpha^4 - 2.22\alpha^3 + 5.19\alpha^2 + 0.18\alpha)$, and (e) $(-0.141\alpha^3 + 2.7\alpha^2 + 0.18\alpha)$.

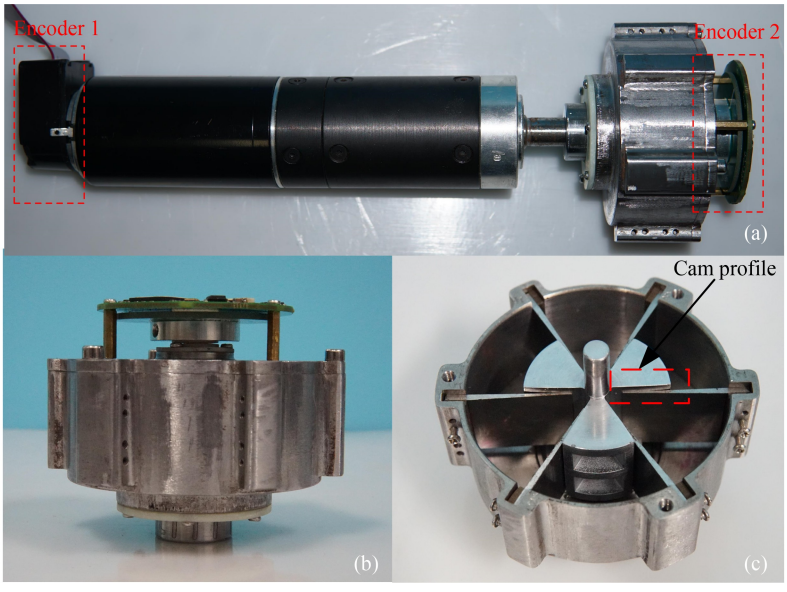

Fig. 10 Prototype of nonlinear stiffness actuator (NSA): (a) NSA prototype, (b) overall structure of nonlinear spring, and (c) internal structure of nonlinear spring.

combining with diverse motors and reducers to act as an NSA, only the specifications of nonlinear spring prototype are detailed in Table 2.

The predefined torque–deflection profile was verified on the NSA prototype by using the setup shown in Fig. 11. The external torque was applied by the motor. Meanwhile, the shells of the motor and the reducer, and the output of the NSA were fixed on the base. A torque sensor (HCNJ-101, 100 N·m) was used to measure the external torque, with its input rigidly connecting the output of the NSA by a coupling and its output rigidly connecting the base. The measured torque and deflection were collected by an STM32F103ZET6 control board and processed by a PC.

As detailed in the previous section, the torque–deflection curve for only one direction is shown here for brevity, as shown in Fig. 12. The experimental curve is close to the predefined profile. In the loading phase, the maximum torque error is −2.2 N·m, and the RMS error is 1.064 N·m. In the unloading phase, the maximum torque error is −4.012 N·m, and the RMS error is 1.773 N·m. The error mainly arises from the material characteristic, machining error, assembly error, and friction force. Specifically, because of heat treatment, the actual Young's modulus of the leaf spring is slightly smaller than the value used in the design process, resulting in the actual torque being smaller than the predefined torque. Due to machining and assembling errors, a clearance exists between the leaf spring and the cam. As a result, guaranteeing that three pairs of leaf springs and cams contact in the desired position perfectly at the same time is difficult, which leads to the experimental torque being smaller than the predefined value. Due to machining error, assembly error, and friction, torque hysteresis occurs in the unloading phase. The hysteresis could be improved by processing methods with high precision, monolithic design of leaf springs and the leaf spring base, and lubrication. For the current prototype, the hysteresis could be eliminated by a compensation algorithm.

Table 2 Specifications of nonlinear spring

Specification	Value
Length	63 mm
Maximum diameter	76 mm
Weight	0.437 kg
Range of deflection	±3°
Range of torque	0–21 N·m
Range of stiffness	0.18–20 N·m/(°)
Range of motion	±180°

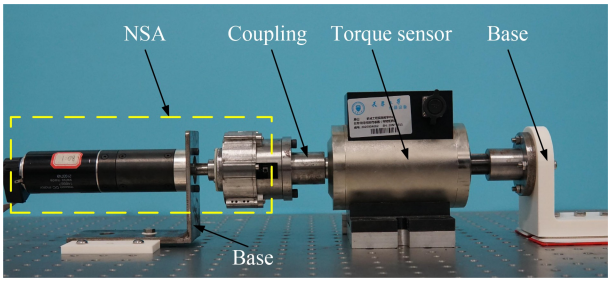

Fig. 11 Experimental setup of the verification experiment of the torque–deflection profile.

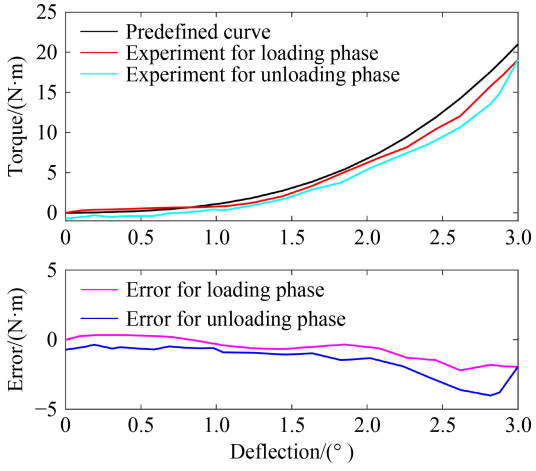

Fig. 12 Results of the verification experiment of the predefined torque–deflection profile.

6.3 Sinusoidal tracking

Torque and position sinusoidal tracking experiments were conducted to evaluate the tracking performance of the new NSA. The torque tracking experiment and the position tracking experiment were carried out in the setup in Fig. 11. A proportion integration differentiation (PID) controller was adopted in the experiments, and feedback was provided by encoders instead of the torque sensor. In the position tracking experiment, the output of the NSA was connected to an inverted pendulum to simulate the load in practical tasks.

Figure 13(a) shows the torque tracking performance for an amplitude of 15 N·m at 1 Hz, where the stiffness variation is 0.18–16 N·m/(°). The tracking trajectory exhibits good accuracy, with a maximum error is 0.506 N·m, and the RMS error is 0.228 N·m. Figures 13(b) and 13(c) show the position tracking performance for an amplitude of 100° under different loads (0 and 2 kg) at 1 Hz. When no load exists on the output, the tracking trajectory exhibits good accuracy, with the maximum error of 1.668° and RMS error of 0.706°. When the load on the output is 2 kg, the maximum error increases to 2.197°, and the RMS error increases to 1.405°, indicating that increasing the load could decrease the position tracking accuracy of the NSA.

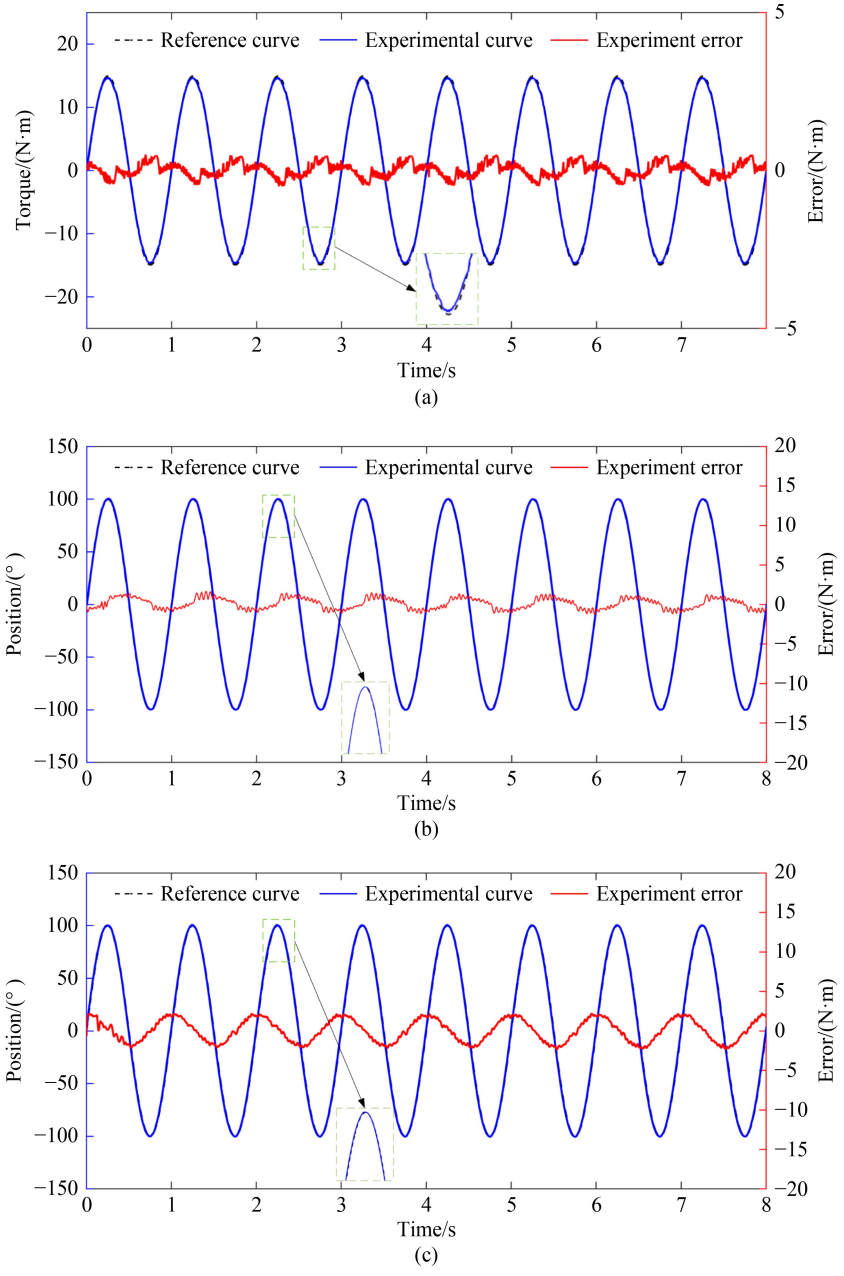

Fig. 13 Experimental results of sinusoidal tracking: (a) torque tracking for an amplitude of 15 N·m at 1 Hz, (b) position tracking for an amplitude of 100° under no load at 1 Hz, and (c) position tracking for an amplitude of 100° under a load of 2 kg at 1 Hz.

6.4 Zero-torque tracking

For evaluation of the interactive performance of the new NSA, a zero-torque tracking experiment was carried out using the setup in Fig. 11 while the output is free and the torque sensor was not used. A rotation was applied to the output manually. A PID controller was also adopted in the experiment. The experimental results are shown in Fig. 14. The torque in the output of the new NSA is close to zero when the output rotates manually, with the RMS error of 0.011 N·m. When the angular speed of the output increases, the error increases but the maximum torque error is 0.025 N·m. The experiment result indicates that

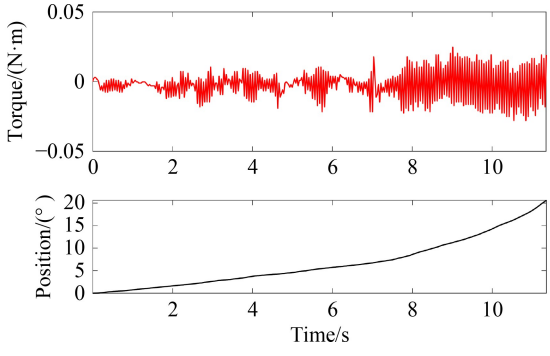

Fig. 14 Experimental results of the zero-torque tracking.

the new NSA has good interactive performance.

7 Discussion

Different from uncontacted interaction between human and robot [53], physical interaction needs compliance in robot joint. This work presents a new simple NSA oriented to engineering applications. The NSA is one kind of compliant actuator that could perform a predefined torque–deflection profile. One contribution of this work is its simple structure. Different from many NSAs with complicated structures, the new NSA adopted a cam-based mechanism without the roller as the basic configuration to realize compact structure and it is lightweight, which are both beneficial for its practical application. Though sliding friction force is inevitable because no rollers were used in the cam-based mechanism, the sliding displacement between the cam and the leaf spring is proven to be very small and the consumption of sliding friction force is very low.

Another contribution of this study is the analytical design method of the NSA, which is precise and efficient for engineering applications. Different from some numerical methods, the study developed an analytical methodology that maps the predefined torque–deflection profile to the profile curve of cam. Moreover, the optimal design parameters of nonlinear spring could be determined by analyzing the mechanics characteristics of leaf spring and the weight of the NSA. The influences of the design parameters on the mechanic characteristic of the leaf spring and the weight of the NSA are unambiguous. Thus, the optimal parameters could be determined efficiently and easily.

The new NSA was compared with other types of NSAs, and the results are shown in Table 3. The new NSA has significant advantages in size and weight. Moreover, for the new NSA, its weight without the motor, namely, the weight of the nonlinear spring, is small, which makes it have great potential for NSA lightweight needs. The deflection range of the new NSA is relatively small compared with that of the HypoSEA, but its stiffness range is clearly advantageous. In particular, because the deflection range of the HypoSEA is very large, its maximum stiffness is considerably smaller than that of the new NSA. The new NSA could fully rotate and inverse, thus its potential to be used for different rotatory joints. The torque range and stiffness range are predefined by users in accordance with specific application scenarios. By setting h_1 as a small value, the new NSA could achieve a small stiffness. By setting h_2 as a big value, the new NSA could achieve a large stiffness. For the nonlinear spring in this study, the ratio between the peak output torque and the weight has a significant advantage, which means a large torque density that is important for wearable robotics. In addition, the weight and length of the new NSA could be further reduced by further optimization.

Several methodological issues should be noted. The first issue is the effect of sliding friction force. Although the influence of sliding friction force is proven small, its effect on the failure of the nonlinear spring should not be neglected. The leaf spring may break because of stress and fatigue. A small R and a small h_1 should be selected to design the NSA to avoid too large stress on the leaf spring, as revealed in Fig. 6(b). Materials with high yield strength could be used to avoid the fatigue of the leaf spring, and its surface quality could be improved. In addition, the leaf spring and the cam surface may be worn, even be glued together, which could be improved by lubrication, improving surface quality, and sealing. The second issue is the assembly error. The verification experiment of the torque–deflection profile and the sinusoidal tracking experiment showed that the assembly error does affect the performance of the NSA. For reduction in the effect of assembly error, except for using processing equipment and methods with high precision, a monolithic part combining leaf springs and leaf spring base could be adopted to guarantee the accuracy of leaf springs and eliminate the clearance between leaf springs and leaf spring base. The last issue is the boundary of the predefined profiles in this study. The new NSA is aimed at monotonically increasing torque–deflection profiles, whose slope is positive and increasing. Although three predefined torque–deflection profiles with different forms of nonlinear stiffness characteristics are proven to be available in the new NSA, those torque–deflection profiles that could lead to too plain cam curve are not suitable.

Table 3 Comparison of different nonlinear stiffness actuators

Nonlinear stiffness actuator	Length/mm	Diameter or width/mm	Weight with motor/kg	Weight without motor/kg	Deflection range/(°)	Range of motion/(°)	Peak output torque/(N·m)	Range of stiffness/(N·m·(°)$^{-1}$)	Ratio between peak output torque and weight without motor/(N·m·kg^{-1})
HypoSEA[a)]	> 600	140	8.900	–	±60.0	–	126	0.00–5.20	–
NSA[b)]	450	250	3.600	3.000	±1.7	±180	36	3.00–77.89	12.00
NSA[c)]	90	180	2.700	0.960	±2.0	±180	22	0.93–36.21	22.92
New NSA	**63**	**76**	**1.445**	**0.437**	±3.0	**±180**	21	0.18–20.00	**46.98**

Notes: a) Refers to Ref. [34], b) refers to Ref. [51], and c) refers to Ref. [52].

8 Conclusions

In this paper, oriented to engineering applications, a new simple NSA was proposed, including leaf springs and especially designed cams, which could perform a predefined torque–deflection profile. The new NSA has a compact structure, and it is lightweight, which are both beneficial for its practical application. An analytical methodology that maps the predefined torque–deflection profile to the cam profile curve was also developed. The weight of the NSA and the mechanic characteristic of the leaf spring were analyzed to obtain the optimal parameters of the structure. The results show that a small R and a small h_1 could lead to lighter weight and stronger overload capacity of the nonlinear spring. As an inevitable issue, the sliding friction force was analyzed, and the results indicate that the sliding displacement between the cam and the leaf spring is very small and consumption of sliding friction force is very low. Simulations of the nonlinear springs with different torque–deflection profiles were performed, and the results show good agreement with the predefined profiles. A prototype with light weight and small size was fabricated, and a verification experiment of the predefined torque–deflection profile was conducted, wherein the experimental curve is close to the predefined profile. The tracking performance and interactive performance of the new NSA are proven to be high by two types of sinusoidal tracking experiments and a zero-torque tracking experiment, respectively. The proposed NSA is promising in the physical interaction between robot and the environment, such as rehabilitation robots, prostheses, exoskeletons, and walking robots. Future studies could focus on the implementation of the new NSA in rehabilitation robotics.

Nomenclature

Abbreviations

NSA	Nonlinear stiffness actuator
PID	Proportion integration differentiation
RMS	Root mean square
SEA	Series elastic actuator
VSA	Variable stiffness actuator

Variables

A_z	Area of the cross section
b	Width of the leaf spring
c	Count of uniform intervals
D_{cam}	Weight of the cam in the cam shaft
E	Young's modulus of the leaf spring
F	Contacting force between the cam and the leaf spring
F_{a}	Axial component of F
F_{n}	Normal force
F_{s}	Sliding friction force
F_{t}	Tangential component of F
G	Shear modulus of the leaf spring
h	Height of the leaf spring
h_1	Height of the free end of the leaf spring
h_2	Height of the fixed end of the leaf spring
I_z	Moment of inertia of the cross section
k_{min}	Minimum stiffness of the NSA
l	Effective length of the leaf spring
l_0	Effective length of the leaf spring on the first contact point
l_m	Effective length of the leaf spring in the mth interval
l_{m-1}	Effective length of the leaf spring in the $(m-1)$th interval
l_{min}	Minimum value of l
L	Length of the leaf spring
m	Sequence number of intervals
M_{max}	Maximum bending moment in the leaf spring
n	Count of leaf springs in a single rotational direction
P_{s}	Power of the sliding friction force
P_τ	Power of the external torque
R	Distance between points O and P
s_{cm}	Length of the cam profile curve in the mth interval
s_{lm}	Effective length variation of the leaf spring in the mth interval
$s_{\tau m}$	Sliding distance of the leaf spring in the mth interval
S_{r}	Accumulated sliding distance of leaf spring
u	Axial offset of the leaf spring
v	Tangential deformation of the leaf spring
v_{s}	Sliding velocity
v_M	Velocity of point M
W	Section modulus on the fixed end of the leaf spring
x_0	Abscissa of the first point on the cam profile curve
x_m	Abscissa of the mth point on the cam profile curve
x_{m-1}	Abscissa of the $(m-1)$th point on the cam profile curve
x_N	Abscissa of point N
$x_{N''}$	Abscissa of point N''
$x_{N_{\text{f}}}$	Abscissa of point N_{f}
y_0	Ordinate of the first point on the cam profile curve
y_m	Ordinate of the mth point on the cam profile curve
y_{m-1}	Ordinate of the $(m-1)$th point on the cam profile curve
y_N	Ordinate of point N
$y_{N''}$	Ordinate of point N''
$y_{N_{\text{f}}}$	Ordinate of point N_{f}
z	Distance of a point to the free end on the leaf spring
α	Deflection of the nonlinear spring

β	Angle between F_a and F_t
θ	Deflection angle of the leaf spring with length l
θ_e	Rotation of output
θ_m	Rotation of motor
μ	Coefficient of sliding friction force
ξ	Coefficient related to the uniform distribution of the shear stress
ρ	Density of cam shaft
σ	Maximum normal stress in the leaf spring
$[\sigma]$	Permissible bending stress of the leaf spring
τ	External torque
τ_{max}	Maximum torque applied to the NSA
ω	Angular velocity of the spring base

Acknowledgements This work was supported by the National Key R&D Program of China (Grant No. 2019YFB1312404) and the National Natural Science Foundation of China (Grant Nos. 51975401 and 51875393). There is no conflict of interest about our work with others.

References

1. Pratt G A, Williamson M M. Series elastic actuators. In: Proceedings of 1995 IEEE/RSJ International Conference on Intelligent Robots and Systems. Human Robot Interaction and Cooperative Robots. Pittsburgh: IEEE, 1995, 399–406
2. Van Ham R, Vanderborght B, Van Damme M, Verrelst B, Lefeber D. MACCEPA, the mechanically adjustable compliance and controllable equilibrium position actuator: design and implementation in a biped robot. Robotics and Autonomous Systems, 2007, 55(10): 761–768
3. Deboon B, Nokleby S, Delfa N L, Rossa C. Differentially-clutched series elastic actuator for robot-aided musculoskeletal rehabilitation. In: Proceedings of 2019 International Conference on Robotics and Automation (ICRA). Montreal: IEEE, 2019, 1507–1513
4. Pfeifer S, Pagel A, Riener R, Vallery H. Actuator with angle-dependent elasticity for biomimetic transfemoral prostheses. IEEE/ASME Transactions on Mechatronics, 2015, 20(3): 1384–1394
5. Aguirre-Ollinger G, Yu H Y. Lower-limb exoskeleton with variable-structure series elastic actuators: phase-synchronized force control for gait asymmetry correction. IEEE Transactions on Robotics, 2021, 37(3): 763–779
6. Van Ham R, Sugar T G, Vanderborght B, Hollander K W, Lefeber D. Compliant actuator designs. IEEE Robotics & Automation Magazine, 2009, 16(3): 81–94
7. Kong K, Bae J, Tomizuka M. A compact rotary series elastic actuator for human assistive systems. IEEE/ASME Transactions on Mechatronics, 2012, 17(2): 288–297
8. Paine N, Mehling J S, Holley J, Radford N A, Johnson J, Fok C L, Sentis L. Actuator control for the NASA-JSC Valkyrie humanoid robot: a decoupled dynamics approach for torque control of series elastic robots. Journal of Field Robotics, 2015, 32(3): 378–396
9. Zhang T, Huang H. Design and control of a series elastic actuator with clutch for hip exoskeleton for precise assistive magnitude and timing control and improved mechanical safety. IEEE/ASME Transactions on Mechatronics, 2019, 24(5): 2215–2226
10. Jung Y, Bae J. Torque control of a series elastic tendon-sheath actuation mechanism. IEEE/ASME Transactions on Mechatronics, 2020, 25(6): 2915–2926
11. Kwak J, Choi W, Lee C, Oh S. Gravity and impedance compensation of body weight support system driven by two series elastic actuators. IEEE/ASME Transactions on Mechatronics, 2021, 27(1): 190–201
12. Liu Y Y, Li Z J, Su H, Su C Y. Whole body control of an autonomous mobile manipulator using series elastic actuators. IEEE/ASME Transactions on Mechatronics, 2021, 26(2): 657–667
13. Pei Y N, Han T Y, Zallek C M, Liu T, Yang L J, Hsiao-Wecksler E T. Design and clinical validation of a robotic ankle-foot simulator with series elastic actuator for ankle clonus assessment training. IEEE Robotics and Automation Letters, 2021, 6(2): 3793–3800
14. Robinson D W. Design and analysis of series elasticity in closed-loop actuator force control. Dissertation for the Doctoral Degree. Cambridge: Massachusetts Institute of Technology, 2000, 18–19
15. Carpino G, Accoto D, Sergi F, Luigi Tagliamonte N L, Guglielmelli E. A novel compact torsional spring for series elastic actuators for assistive wearable robots. Journal of Mechanical Design, 2012, 134(12): 121002
16. Paine N, Oh S, Sentis L. Design and control considerations for high-performance series elastic actuators. IEEE/ASME Transactions on Mechatronics, 2014, 19(3): 1080–1091
17. Tsagarakis N G, Sardellitti I, Caldwell D G. A new variable stiffness actuator (CompAct-VSA): design and modelling. In: Proceedings of 2011 IEEE/RSJ International Conference on Intelligent Robots and Systems. San Francisco: IEEE, 2011, 378–383
18. Wolf S, Eiberger O, Hirzinger G. The DLR FSJ: energy based design of a variable stiffness joint. In: Proceedings of 2011 IEEE International Conference on Robotics and Automation. Shanghai: IEEE, 2011, 5082–5089
19. Choi J, Hong S, Lee W, Kang S, Kim M. A robot joint with variable stiffness using leaf springs. IEEE Transactions on Robotics, 2011, 27(2): 229–238
20. Jafari A, Tsagarakis N G, Caldwell D G. A novel intrinsically energy efficient actuator with adjustable stiffness (AwAS). IEEE/ASME Transactions on Mechatronics, 2013, 18(1): 355–365
21. Liu Y W, Cui S P, Sun Y J. Mechanical design and analysis of a novel variable stiffness actuator with symmetrical pivot adjustment. Frontiers of Mechanical Engineering, 2021, 16(4): 711–725
22. Sun J T, Guo Z, Sun D Y, He S Y, Xiao X H. Design, modeling and control of a novel compact, energy-efficient, and rotational serial variable stiffness actuator (SVSA-II). Mechanism and Machine Theory, 2018, 130: 123–136
23. Wu J H, Wang Z R, Chen W, Wang Y Q, Liu Y H. Design and validation of a novel leaf spring-based variable stiffness joint with reconfigurability. IEEE/ASME Transactions on Mechatronics,

2020, 25(4): 2045–2053

24. Zhu Y H, Wu Q C, Chen B, Xu D W, Shao Z Y. Design and evaluation of a novel torque-controllable variable stiffness actuator with reconfigurability. IEEE/ASME Transactions on Mechatronics, 2021, 27(1): 292–303
25. Xu Y P, Guo K, Sun J, Li J F. Design, modeling and control of a reconfigurable variable stiffness actuator. Mechanical Systems and Signal Processing, 2021, 160: 107883
26. Sun Y X, Tang P, Dong D B, Zheng J, Chen X H, Bai L. Modeling and experimental evaluation of a pneumatic variable stiffness actuator. IEEE/ASME Transactions on Mechatronics, 2022, 27(5): 2462–2473
27. Mengacci R, Garabini M, Grioli G, Catalano M G, Bicchi A. Overcoming the torque/stiffness range tradeoff in antagonistic variable stiffness actuators. IEEE/ASME Transactions on Mechatronics, 2021, 26(6): 3186–3197
28. Li X, Zhu H Y, Lin W, Chen W J, Low K H. Structure-controlled variable stiffness robotic joint based on multiple rotary flexure hinges. IEEE Transactions on Industrial Electronics, 2021, 68(12): 12452–12461
29. Yang S K, Chen P, Wang D Q, Yu Y, Liu Y W. Design and analysis of a 2-DOF actuator with variable stiffness based on leaf springs. Journal of Bionic Engineering, 2022, 19: 1392–1404
30. Liu L, Misgeld B J E, Pomprapa A, Leonhardt S. A testable robust stability framework for the variable impedance control of 1-DOF exoskeleton with variable stiffness actuator. IEEE Transactions on Control Systems Technology, 2021, 29(6): 2728–2737
31. Koganezawa K, Watanabe Y, Shimizu N. Antagonistic muscle-like actuator and its application to multi-d.o.f. forearm prosthesis. Advanced Robotics, 1997, 12(7–8): 771–789
32. Hollander K W, Sugar T G, Herring D E. Adjustable robotic tendon using a 'Jack Spring'/spl trade/. In: Proceedings of the 9th International Conference on Rehabilitation Robotics. Chicago: IEEE, 2005, 113–118
33. Hutter M, David C D, Siegwart R. Design of an articulated robotic leg with nonlinear series elastic actuation. In: Tosun O, Akin H L, Tokhi M O, Virk G S, eds. Mobile Robotics: Solutions and Challenges. New Jersey: World Scientific, 2009, 645–652
34. Thorson I, Caldwell D. A nonlinear series elastic actuator for highly dynamic motions. In: Proceedings of 2011 IEEE/RSJ International Conference on Intelligent Robots and Systems. San Francisco: IEEE, 2011, 390–394
35. Chen W H, Zhou L B, Wang J H, Zhao Z, Chen W J, Bai S P. A Maxwell-slip based hysteresis model for nonlinear stiffness compliant actuators. IEEE Transactions on Industrial Electronics, 2021, 69(11): 11510–11520
36. Rodríguez A G, Chacón J M, Donoso A, González Rodríguez A G. Design of an adjustable-stiffness spring: mathematical modeling and simulation, fabrication and experimental validation. Mechanism and Machine Theory, 2011, 46(12): 1970–1979
37. Li B K, Hao G B. Nonlinear behaviour design using the kinematic singularity of a general type of double-slider four-bar linkage. Mechanism and Machine Theory, 2018, 129: 106–130
38. Liu Y W, Wang D Q, Yang S K, Liu J G, Hao G B. Design and experimental study of a passive power-source-free stiffness-self-adjustable mechanism. Frontiers of Mechanical Engineering, 2021, 16(1): 32–45
39. Li Z Y, Bai S P, Chen W H, Zhang J B. Nonlinear stiffness analysis of spring-loaded inverted slider crank mechanisms with a unified model. Journal of Mechanisms and Robotics, 2020, 12(3): 031011
40. Migliore S A, Brown E A, DeWeerth S P. Biologically inspired joint stiffness control. In: Proceedings of the 2005 IEEE International Conference on Robotics and Automation. Barcelona: IEEE, 2005, 4508–4513
41. Shao Y X, Zhang W X, Su Y J, Ding X L. Design and optimisation of load-adaptive actuator with variable stiffness for compact ankle exoskeleton. Mechanism and Machine Theory, 2021, 161: 104323
42. Hao G B. A framework of designing compliant mechanisms with nonlinear stiffness characteristics. Microsystem Technologies, 2018, 24(4): 1795–1802
43. Palli G, Berselli G, Melchiorri C, Vassura G. Design of a variable stiffness actuator based on flexures. Journal of Mechanisms and Robotics, 2011, 3(3): 034501
44. Radaelli G, Herder J L. Shape optimization and sensitivity of compliant beams for prescribed load-displacement response. Mechanical Sciences, 2016, 7(2): 219–232
45. Schepelmann A, Geberth K A, Geyer H. Compact nonlinear springs with user defined torque-deflection profiles for series elastic actuators. In: Proceedings of 2014 IEEE International Conference on Robotics and Automation (ICRA). Hong Kong: IEEE, 2014, 3411–3416
46. Kuo P H, Deshpande A D. A novel joint design for robotic hands with humanlike nonlinear compliance. Journal of Mechanisms and Robotics, 2016, 8(2): 021004
47. Bi S S, Qiao T, Zhao H Z, Yu J J. Stiffness analysis of two compliant pivots used in series elastic actuators. Transactions of the Canadian Society for Mechanical Engineering, 2012, 36(3): 315–328
48. Kuo P H, Deshpande A D. Muscle-tendon units provide limited contributions to the passive stiffness of the index finger metacarpophalangeal joint. Journal of Biomechanics, 2012, 45(15): 2531–2538
49. Lan S B, Song Z B. Design of a new nonlinear stiffness compliant actuator and its error compensation method. Journal of Robotics, 2016, 2016: 7326905
50. Zhao Y R, Song Z B, Ma T Y, Dai J S. Optimisation of stiffness to achieve increased bandwidth and torque resolution in nonlinear stiffness actuators. IEEE Transactions on Industrial Electronics, 2020, 67(4): 2925–2935
51. Song Z B, Lan S B, Dai J S. A new mechanical design method of compliant actuators with non-linear stiffness with predefined deflection-torque profiles. Mechanism and Machine Theory, 2019, 133: 164–178
52. Hu X Q, Song Z B, Ma T Y. Novel design method for nonlinear stiffness actuator with user-defined deflection-torque profiles. Mechanism and Machine Theory, 2020, 146: 103712
53. Qi K K, Song Z B, Dai J S. Safe physical human-robot interaction: a quasi whole-body sensing method based on novel laser-ranging sensor ring pairs. Robotics and Computer-Integrated Manufacturing, 2022, 75: 102280